ACS OMEGA

http://pubs.acs.org/journal/acsodf

Article

Insight into the Effect of Sulfonation Techniques on the Adsorption Properties of $-SO_3H$ Surface-Functionalized Coal as Adsorbent for Malachite Green Dye: Steric and Energetic Investigation

Ali A. AlHammadi, Rania Nasser, Mohamed S. Shaban, Sarah I. Othman, Jong Seong Khim, Jamaan S. Ajarem, Ahmed A. Allam, and Mostafa R. Abukhadra*

Cite This: *ACS Omega* 2022, 7, 36697−36711

Read Online

ACCESS | Metrics & More | Article Recommendations | Supporting Information

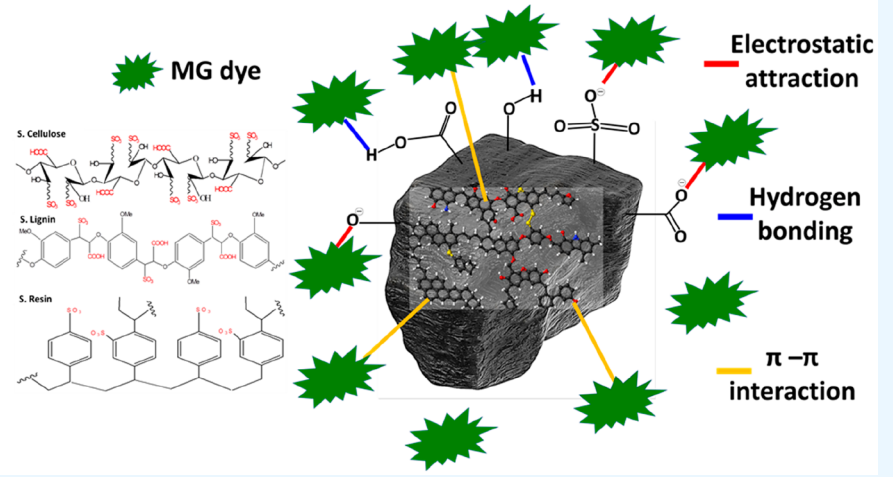

ABSTRACT: Natural coal (N.C) was sulfonated with sulfuric acid by normal stirring (MS.C) and sonication waves (SS.C) to obtain $-SO_3H$ functionalized coal as enhanced adsorbents of malachite green dye (MG). The sulfonated products exhibit enhanced surface area (MS.C (27.2 m^2/g) and SS.C (45.8 m^2/g)) as compared to N.C. SS.C achieved higher acid density (14.2 mmol/g) and sulfur content (13.2 wt. %) as compared to MS.C. The impact of the sulfonation processes on the adsorption of MG was assessed based on the monolayer isotherm model of one energy. The MG Q_{sat} of N.C (121.3 mg/g), MS.C (226.3 mg/g), and SS.C (296.4 mg/g) validate the significant effect of the sulfonation processes by the sonication waves. This is in agreement with the active site densities that reflect the saturation of SS.C by more active sites (180.74 mg/g) than MS.C (120.38 mg/g) and N.C (70.84 mg/g). The MS.C and SS.C can adsorb three MG molecules as compared to two molecules per site of N.C. The Gaussian energy (<8 kJ/mol) and adsorption energy (<40 kJ/mol)) reflects the physisorption of MG involving van der Waals forces, hydrogen bonding, and dipole bonding forces. The thermodynamic functions demonstrate the uptake of MG by exothermic, spontaneous, feasible reactions.

INTRODUCTION

The water contamination phenomenon represents the most critical concern that threatens strongly the safety of the contemporary world and the healthy life of the population.[1,2] The discharged quantities of sewage water and industrial wastewater increased strongly at an uncontrolled rate as a result of the extensive increase in agricultural, mining, industrial, and overpopulation activities.[3] Numerous types of dissolved organic (pharmaceutical residuals, dyes, pesticides, and petrochemicals) and inorganic species (heavy metals, phosphate, ammonium, sulfate, and nitrate) were identified as water pollutants of remarkable health and environmental side impacts.[2−5]

Synthetic dyes were introduced into the industrial communities as a vital aromatic for different applications. However, most of the commonly used dyes exhibit the chemical structure of significant biodegradable resistance and toxicity.[6,7] Moreover, their discharge (7×10^5 tons per year) into fresh water is associated with some health problems such as cancer, dermatitis, allergies, skin irritation, and kidney

Received: August 5, 2022
Accepted: September 29, 2022
Published: October 7, 2022

damage.[8,9] Environmentally, the existence of such synthetic organic structures in the water systems causes significant disruption to the bioactivity and photosynthesis activity of the aquatic organisms by blocking the penetration efficiency of the sunlight.[9,10] Among the commonly studied dyes malachite green ($C_{23}H_{26}N_2OCI_{42}$) (MG) is a widely detected synthetic dye in water resources. However, MG dye is of wide applications in food, aquaculture, and medical disinfectant industries, it was classified as a highly toxic compound.[10,11] Carcinogenesis, mutagenesis, chromosomal fractures, respiratory toxicity, and teratogenicity were identified as health side effects and diseases related to the MG contaminated water.[12,13] Considering the previous environmental and health issues, the decolorization of such synthetic dyes is a critical challenge for the researchers and responsible authorities.

Therefore, the decolorization of the dye molecules by low-cost and innovative techniques was investigated recently in several studies recently.[14,15] The adsorption processes as a decolorization technique of the dissolved synthetic dyes were endorsed strongly for their high efficiency, simplicity, recyclability, and production cost considerations as compared to the other investigated methods including filtration, ion exchange processes, chemical precipitation, and coagulation.[16,17] Availability, fabrication cost, recyclability, biodegradability, safety, and adsorption capacity are the main parameter that controls the suitability of the selected adsorbent and its efficiency.[18] Recently, natural-based carbonaceous materials and raw coal were assessed widely as potential adsorbents of some synthetic dyes as well as other types of dissolved chemicals.[19−22] The raw coal was applied effectively in the removal of some synthetic dyes such as methylene blue,[20] methyl orange,[23] basic blue 3 (BB3) dye,[24] and basic yellow 2 (BY2) dye.[24]

As a geological term, coal refers to a sedimentary rock of high worldwide natural reserves and is composed of different types of organic components (cellulose, resin, lignite, and macerals) and inorganic ashes.[22,25,26] As a material, it was identified as a series of natural polycyclic aromatic hydrocarbons, and the aromatic rings in its structure are linked with each other by types of oxygen-bearing functional groups (carbonyl, carboxyl, phenolic, and hydroxyl groups).[27,28] The existence of such active oxygen-bearing chemical groups, especially the carboxylic and phenolic groups, makes it a promising adsorbent for different species of water-dissolved chemical compounds.[29] The previous studies demonstrate that the physicochemical properties of coals as adsorbents depend essentially on their surface properties such as the dominant chemical groups, surface area, and porosity properties.[22,30] Therefore, several studies were introduced to follow the impact of the different surface modification processes on the chemical and textural properties of coal. Such modification processes involved demineralization, chemical activation, metal loading, and thermal activation of coal fractions.[19,22]

The chemical activation of coal and carbonaceous materials is the most applied technique to support their surfaces by additional or new active chemical groups especially the oxygenated chemical groups such as the hydroxyl groups (−OH) and carboxyl groups (−COOH).[20,31] The sulfonation of coal was reported as a very effective method that can support its structure by different active oxygenated chemical groups in addition to the significant enhancement in its surface electronegativity.[19,20,31] The sulfonation efficiency and the physicochemical properties of the modified coal as adsorbent depend essentially on the type of the used chemical activators, the activation conditions, and the used activation techniques.[28,32] The sulfonation of coal as an acidic heterogeneous catalyst by sulfuric acid (H_2SO_4) as cost-effective and highly oxidizing acid resulted in a significant enhancement in its acid density and textural properties during its application in the transesterification reactions.[30] Moreover, conducting the sulfonation reactions under the sonication source resulted in different surficial properties than the sulfonated product by normal stirring processes.[19,32,33]

Unfortunately, the adsorption properties of sulfonated raw coal were not covered by the satisfied studies yet considering the sulfonation agent, sulfonation conditions, sulfonation techniques, and types of dissolved chemical contaminants. The sulfonation of raw coal without precarbonization processes will result in enhanced low-cost adsorbent of numerous active functional groups and high adsorption capacities to be used effectively in the decontamination of organic pollutants. Also, advanced mixing techniques such as ultrasonic methods can induce the entrapping efficiency of the effective oxygenated chemical groups as well as the surface area of the modified coal as potential adsorbents of significant capacities. Therefore, the introduced study involved a detailed investigation of the adsorption properties of two sulfonated coal products prepared by two activation techniques (normal stirring and sonication) for malachite green basic dye. The adsorption studies were accomplished considering all the experimental variables, classic kinetic studies, traditional equilibrium modeling, and advanced equilibrium model based on the statistical physics theory. The change in the adsorption properties will be assessed based on steric parameters (occupied active sites, number of adsorbed dyes molecules by site, and saturation adsorption capacities of the sulfonated coal) in addition to the energetic parameters (adsorption energies, internal energy, enthalpy, and entropy).

2. RESULTS AND DISCUSSION

2.1. Characterization of the Studied Adsorbents. The XRD patterns of raw coal as well as the sulfonated samples demonstrate considerable changes in the structures after the sulfonation reactions (Figure 1). The obtained XRD pattern of coal precursor reflects the amorphous structure that is related

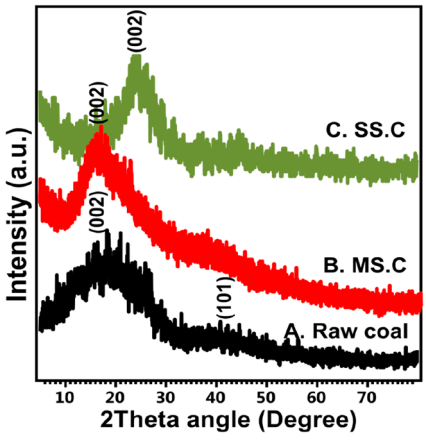

Figure 1. XRD patterns of raw coal (A), sulfonated coal by magnetic stirring (MS.C) (B), and sulfonated coal by sonication waves (SS.C) (C).

https://doi.org/10.1021/acsomega.2c04985
ACS Omega 2022, 7, 36697−36711

to the aromatic sheets of the structural carbon of the coal. This was identified based on the identified broad peaks from 8 to 30° (002) and from 40 to 50° (101) (Figure 1A).[34,35] For the sulfonated samples, the resulting pattern shows a remarkable deviation of the identified main peaks (10−30° for MS.C (Figure 1B) and 15−36° for SS.C (Figure 1C)) to be in higher positions as compared to the raw sample. This suggests strong structural changes after the sulfonation reactions and a significant increase in the amorphization properties of the coal. Such structural impacts are credited to the destructive effect of the sulfuric acid on the C−O−C bonds in addition to its dehydration impact on the carbon-bearing functional groups.[34,36]

The changes in the chemical properties and the formed groups during the sulfonation reactions were followed based on the FT-IR spectra (Figure 2). The identified structural

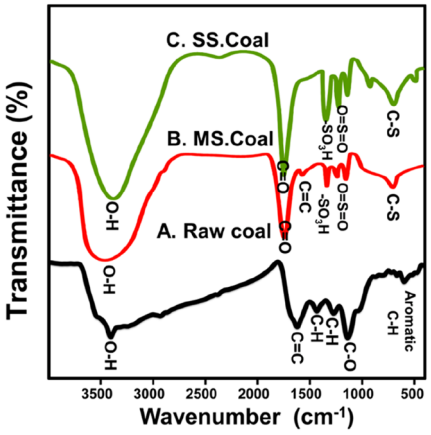

Figure 2. FT-IR spectra of raw coal (A), modified MS.C product (B), and modified SS.C product (C).

groups of the studied coals are phenolic O−H (3403 cm^{-1}), symmetric aliphatic C−H (2858 cm^{-1}), asymmetric aliphatic C−H (2930 cm^{-1}), C═C (1620 cm^{-1}), carboxylic OH and/or C−H of a methylene group (1432 cm^{-1}), C−H of the methyl group (1302 cm^{-1}), C−O (1000−1300 cm^{-1}), and distorted C−H of the aromatic planes (500−900 cm^{-1}) (Figure 2A).[22,25] Regarding the spectrum of MS.C, the increase in the intensity and broadness of the OH identification bands (3398 cm^{-1}) and the identified C = O bond of the carboxylic group (1712 cm^{-1}) reflect the formation of COOH groups as oxidized products during the sulfonation reactions (Figure 2B).[35,37] The existence of sulfur-bearing chemical groups was detected by the SO_3 stretching of $-SO_3H$ (1133 cm^{-1}), symmetric O═S═O (1025 cm^{-1}), asymmetric O═S═O (1001 cm^{-1}), and C−S groups (578 cm^{-1}) (Figure 2B).[28,37] The oxidation and deformation effect of sulfonation reactions on the methyl groups and cellulose components appeared in the remarkable reduction of the identification bands of C═C (1610 cm^{-1}) and C−H (1304 cm^{-1}).[34,36] The same observations were detected for the SS.C sample but with a significant increase in the intensity of the sulfur-bearing functional groups, and the COOH group suggested a higher impact on the sulfonation reactions in the existence of the sonication waves (Figure 2C). This was supported by the estimated analysis of the samples as the coal exhibited a significant increment in the sulfur and oxygen content after the sulfonation reactions, especially in the existence of the sonication waves.

The effect of the sulfonation reaction on the surficial features was studied based on the SEM images (Figure 3). The coal precursor appeared as agglomerated particles composed of several compacted layers that are of massive form and random orientation (Figure 3A). The layered structure is related to the compacted wood tissues and macerals as the main components of the studied sub-bituminous sample. The obtained particles of MS.C exhibit different surfaces of rugged topography with numerous micro nudes and micropores that might be related to the dissolved inorganic components during reactions with H_2SO_4 (Figure 3, parts B and C). Regarding the SEM images of SS.C, the images demonstrated a significant disintegration effect for the sonication waves on the coal grain into smaller particles. Also, there is a remarkable detection of tabular or

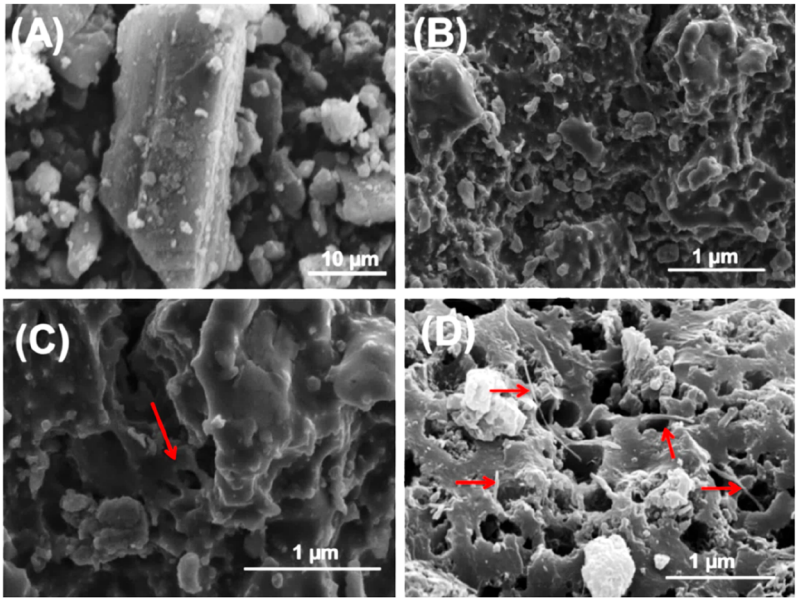

Figure 3. SEM images of raw coal (A), modified MS.C product (B and C), and modified SS.C product (D).

https://doi.org/10.1021/acsomega.2c04985
ACS Omega 2022, 7, 36697−36711

needle-like particles related to the separation of some of the present macerals (liptinite) from the coal layers (Figure 3D). The disintegrated particles still exhibit rugged topography and enhanced porosity as compared to raw coal and MS.C. Such morphological features affected strongly the determined surface area of the products as presented in Table 1. The SS.C sample exhibits a surface area of 45.8 m^2/g which is higher than the determined value for MS.C (27.2 m^2/g).

Table 1. Chemical Composition, Acid Density, and Surface Area of N.Coal, MS.C, and SS.C samples

	N.Coal	MS.C	SS.C
C (wt. %)	68.4	50.2	33.1
S (wt. %)	2.32	7.6	13.2
N (wt %)	2.53	7.8	10.1
H (wt %)	6.3	10.8	14.2
O (wt %)	10.6	24.4	29.3
acid density (mmol/g)	0.064	8.87	14.2
surface area (m^2/g)	5.4	27.2	45.8
av pore diameter	50.2	44.2	23.6

2.2. Adsorption of MG Dye. *2.2.1. Effect of pH.* Adjusting the pH value of the prepared aqueous solutions affects strongly the properties of the adsorption reactions either by directing the ionization speciation of the dissolved compounds or the surface charges of the coal products. Investigation of the effect of pH as a variable during the conducted adsorption tests of MG molecules by N.C, MS.C, and SS.C was followed from pH 2 up to pH 9. The other experimental variables were selected to be at 240 min (contact time), 0.25 g/L (coal dosage), 100 mg/L (dye concentration), 293 K (temperature), and 200 mL (volume). The determined MG adsorption efficiencies by N.C, MS.C, and SS.C exhibit noticeable enhancement with the regular rise in the solution pH up to the highest tested value (pH 9). The MG adsorbed quantities by N.C, MS.C, and SS.C at pH 9 are 45.8, 60.2, and 72.5 mg/g, respectively (Figure 4).

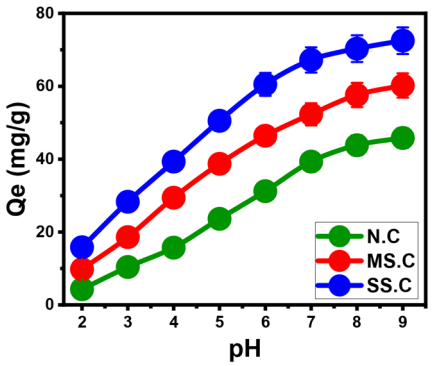

Figure 4. Influence of solutions pH on the adsorption of MG dye by N.C, MS.C, and SS.C (240 min (contact time), 0.25 g/L (coal dosage), 100 mg/L (dye concentration), 293 K (temperature), and 200 mL (volume)).

This was ascribed to the dominant charges on the surfaces of N.C, MS.C, and SS.C particles as well as the ionization properties of MG molecules that exhibit positive charges within the assessed pH range.[38]

The main chemical groups of the raw coal and sulfonated coal products are affected by strong deprotonation reactions under the basic environment which create numerous hydroxyl ions of negative charges. Therefore, the basic conditions during the adsorption of the dyes keep the surfaces of the coal products with numerous negative charges, which are a favorable state for the significant electrostatic attractions of MG molecules that are of positive charges.[39,40] This was supported by the determined $pH_{(ZPC)}$ values of N.C (6.2), MS.C (5.7), and SS.C (5.2) that demonstrate the high saturation of their surface s with negative charges beyond these values. Therefore, pH 9 was selected to conduct the further MG adsorption tests either by N.C, MS.C, and SS.C.

2.2.2. Kinetic Studies. 2.2.2.1. Time Interval. The MG adsorption behaviors in the presence of N.C, MS.C, and SS.C as adsorbents were followed considering different contact intervals from 30 min up to 960 min. The other experimental variables were selected to be at pH 9 (pH of the solutions), 0.25 g/L (coal dosage), 100 mg/L (dyes concentration), 293 K (temperature), and 200 mL (volume). The recognized MG uptake curves by N.C, MS.C, and SS.C reveal a noticeable segmental shape which normally signifies remarkable changes in the actual MG uptake rates with expanding the contact intervals (Figure 5A). The first observed segments or sections in the curves exhibit remarkable steep slopes signifying the fast adsorption rates of MG and strong escalation in its adsorbed quantities by the N.C, MS.C, and SS.C samples with increasing the assessed contact intervals (Figure 5A). The previously described segments were identified up to 540 min for N.C, MS.C, and SS.C. The second MG uptake segments were observed within the tested range from the previously reported contact intervals up to 960 min. During these states, the actual adsorption of MG by N.C, MS.C, and SS.C occurred at remarkable slow rates with a faint or neglected increase in their adsorbed quantities (Figure 5A). Such adsorption rates and behaviors reflect the equilibration states of N.C, MS.C, and SS.C as the used adsorbents of MG dye. The detected MG uptake equilibrium capacities by N.C, MS.C, and SS.C are 71.8, 93.6, and 113.3 mg/g, respectively (Figure 5A). The previously reported MG adsorption behaviors were ascribed to the regular and continuous adsorption of the dyes by the distributed free adsorption receptors on the N.C, MS.C, and SS.C particles with time. Subsequently, the quantities or the numbers of these receptors decline frequently with expanding tested contact intervals causing a diminution in the MG uptake rates by N.C, MS.C, and SS.C particles. After specific contact intervals, all the present receptor sites on the surfaces of N.C, MS.C, and SS.C particles were occupied or consumed by MG as adsorbed molecules and in turn, the modified coal products attend their actual or experimental equilibrium states and they cannot adsorb more dyes molecules.[41]

2.2.2.2. Intraparticle Diffusion Behavior. The intraparticle diffusion curves of MG adsorption processes by N.C, MS.C, and SS.C adsorbents include three obvious sections or segments that exhibit different slopes without detectable crossings through the original points (Figure 5B). This validates the operation of more than one MG uptake mechanism during its adsorption by N.C, MS.C, and SS.C rather than the diffusion of its molecules to be in contact with the surfaces of the coal products.[3] The perfect segmentation of the curves into three sections suggested essential changes in the MG uptake mechanisms by expanding the evaluated contact intervals (Figure 5B). The starting section during the initial contact intervals reflects the impact of the surficial or external MG adsorption processes by N.C, MS.C, and SS.C considering their surficial active groups. After certain intervals,

https://doi.org/10.1021/acsomega.2c04985
ACS Omega 2022, 7, 36697−36711

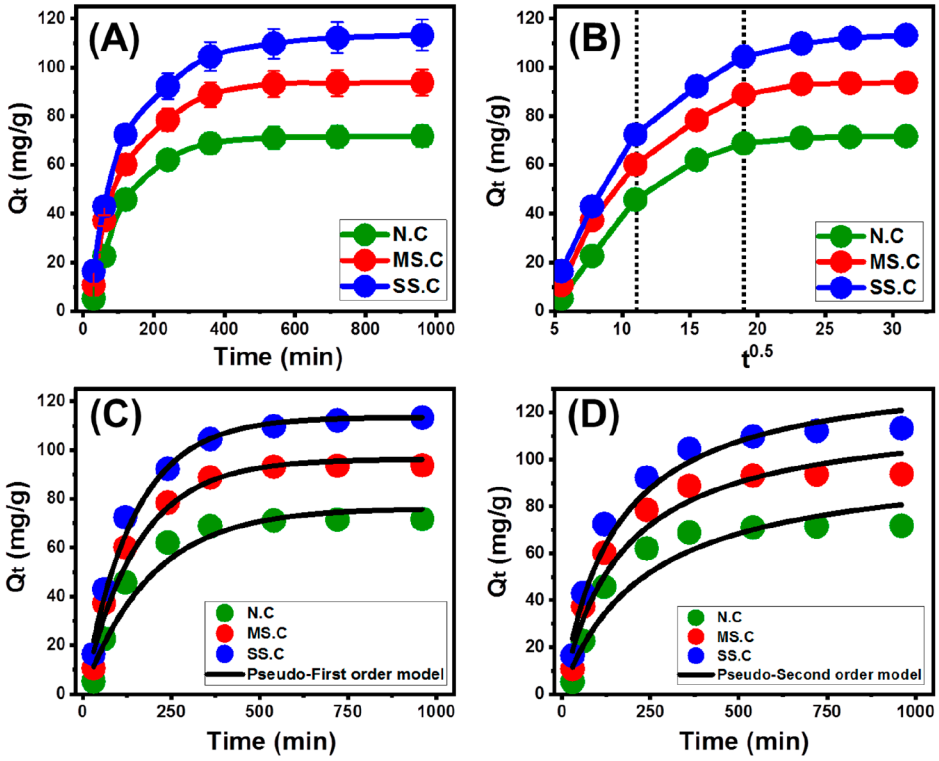

Figure 5. Effect of the time intervals on the on the adsorption of MG by N.C, MS.C, and SS.C (A), the intraparticle diffusion curves of the MG adsorption processes (B), fitting of the MG adsorption results with pseudo-first-order kinetics (C), and fitting of the MG adsorption results with pseudo-second order kinetics (D) (pH 9 (pH of the solutions), 0.25 g/L (coal dosage), 100 mg/L (dyes concentration), 293 K (temperature), and 200 mL (volume)).

the detection of the second sections of the curves reflects a strong fading of the impact of the external MG uptake mechanisms and the operation of another mechanism which is known as layered adsorption mechanisms[42] (Figure 5B). The third section which appeared by the end of the adsorption tests and represents the equilibrium parts of the curves suggested the formation of thick layers of the adsorbed MG on the surfaces of N.C, MS.C, and SS.C (Figure 5B). Additionally, the realization of this section reveals the occurrence of interionic attraction or molecular association or both of them as the controlling MG adsorption mechanisms.[18]

2.2.2.3. Kinetic Modeling. The kinetic modeling of the MG adsorption systems by N.C, MS.C, and SS.C as the applied adsorbents was performed based on the nonlinear fitting results with the reported hypothetical kinetic of pseudo-first-order (Figure 5C) as well as pseudo-second-order models (Figure 5D). The R^2 and χ^2 values were used to detect the fitting degrees of MG adsorption behaviors with the assessed kinetic models (Figure 5, parts C and D; Table 2). According to the fitting parameters, the MG uptake processes by N.C, MS.C, and SS.C follow the kinetic behaviors of the pseudo-first-order hypothesis rather than the pseudo-second-order hypothesis (Table 2; Figure 5, parts C and D). This signifies the dominant influence of the common physisorption mechanisms during the performed adsorption reactions of MG by N.C, MS.C, and SS.C.[43,44] The significant fitting degrees between the MG uptake behaviors and the assumptions of both presented models validate the considerable role of the weak chemisorption processes (chemical complexes and/or ion exchange) as assistant mechanisms during the physisorption uptake of MG by N.C, MS.C, and SS.C.

Table 2. Mathematical Parameters of the Studied Kinetic Models

	kinetic models		
	model	parameters	
N.C	pseudo-first-order	K_1(1/min)	0.0052
		$Q_{e(Cal)}$(mg/g)	76.2
		R^2	0.95
		X^2	1.7
	pseudo-second-order	k_2(mg/g min)	4.29×10^{-5}
		$Q_{e(Cal)}$(mg/g)	100.2
		R^2	0.93
		X^2	2.4
MS.C	pseudo-first-order	K_1(1/min)	0.0065
		$Q_{e(Cal)}$(mg/g)	96.3
		R^2	0.97
		X^2	1.01
	pseudo-second-order	k_2(mg/g min)	4.94×10^{-5}
		$Q_{e(Cal)}$(mg/g)	120.54
		R^2	0.95
		X^2	1.68
SS.C	pseudo-first-order	K_1(1/min)	0.0071
		$Q_{e(Cal)}$(mg/g)	113.48
		R^2	0.98
		X^2	0.47
	pseudo-second-order	k_2(mg/g min)	4.84×10^{-5}
		$Q_{e(Cal)}$(mg/g)	139.6
		R^2	0.97
		X^2	0.99

2.2.3. Equilibrium Studies. 2.2.3.1. Effect of MG Concentration. Conducting the MG uptake tests considering different

https://doi.org/10.1021/acsomega.2c04985
ACS Omega 2022, 7, 36697−36711

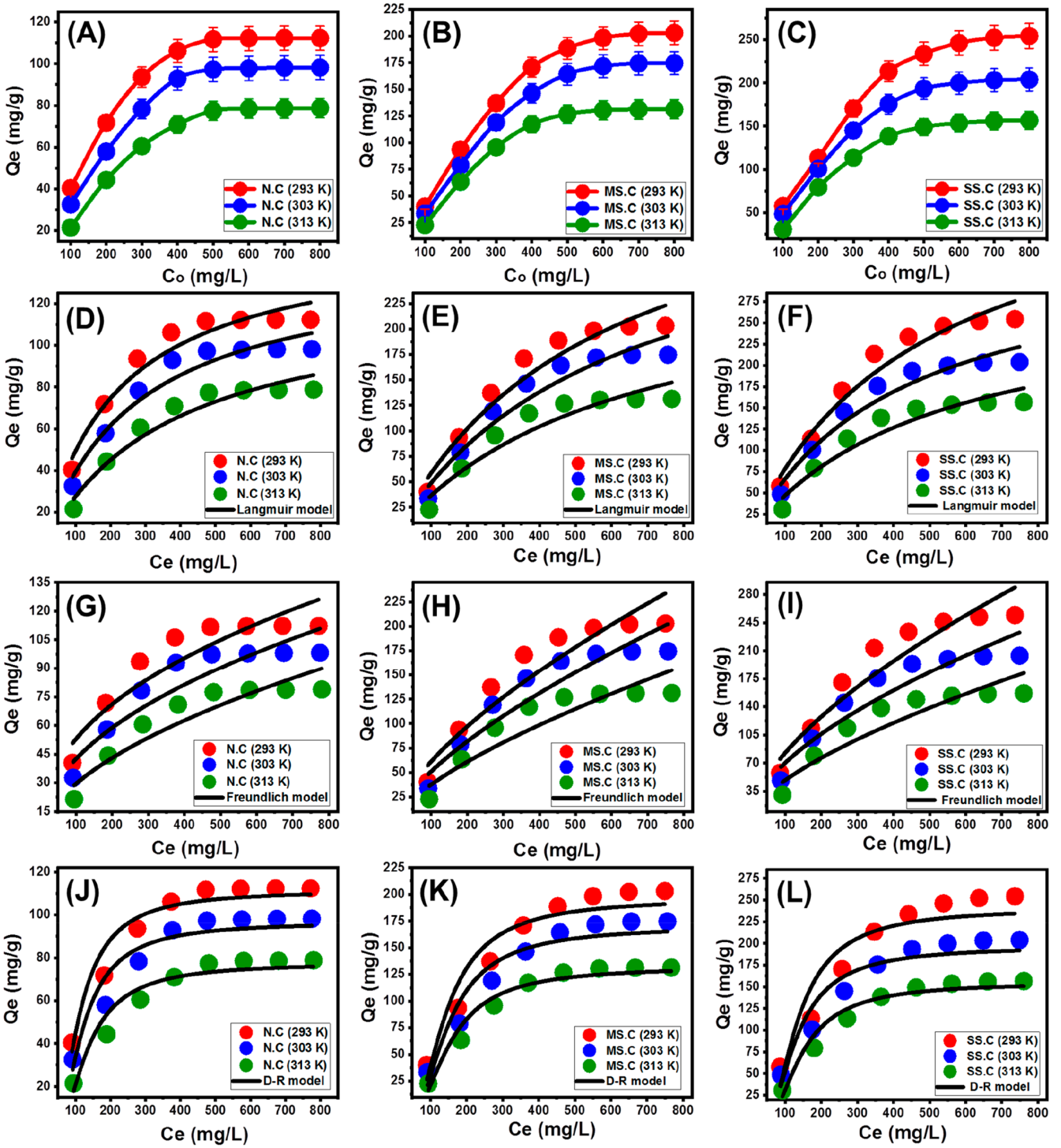

Figure 6. Effect of the MG concentration on its uptake capacities by N.C (A), MS.C (B), and SS.C adsorbents (C), the fitting of the MG adsorption results with the Langmuir model (D−F), fitting of the MG adsorption results with the Freundlich model (G−I), and fitting of the MG adsorption results with the D-R model (J−L) (pH 9 (pH of the solutions), at 0.25 g/L (coal dosage), 780 min (contact time), and 200 mL (volume)).

starting concentrations of its dissolved molecules (100 up to 800 mg/L) can be denoted its maximum adsorbed quantities by N.C, MS.C, and SS.C and the equilibrium properties of the reactions. The other experimental variables were selected to be at pH 9 (pH of the solutions), 0.25 g/L (coal dosage), 780 min (contact time), and 200 mL (volume) considering three values for the adjusted temperature (293, 303, and 313 K). The adsorbed quantities of MG molecules by N.C, MS.C, and SS.C depend strongly on the starting dye concentrations (Figure 6, parts A−C). The high MG concentrations induce the efficiencies of the N.C, MS.C, and SS.C particles as the evaluated solid adsorbents. The previous literature illustrated this experimental behavior as a result of the predicted acceleration in the MG driving forces and/or diffusion speed

https://doi.org/10.1021/acsomega.2c04985
ACS Omega 2022, 7, 36697−36711

Table 3. Mathematical Parameters of the Addressed Kinetic and Classic Isotherm Models

		isotherm models			
	model	parameters	293.13 K	303.13 K	313.13 K
N.C	Langmuir model	Q_{max}(mg/g)	153.37	141.25	124.4
		b (L/mg)	0.0047	0.0038	0.0028
		R^2	0.96	0.96	0.96
		X^2	0.48	0.48	0.53
	Freundlich model	$1/n$	0.42	0.46	0.54
		k_F(mg/g)	7.52	4.93	2.44
		R^2	0.89	0.90	0.90
		X^2	1.48	1.35	1.3
	D-R model	β (mol^2/KJ^2)	0.0376	0.0436	0.0546
		Q_m(mg/g)	111.2	96.6	77.53
		R^2	0.95	0.94	0.95
		X^2	0.58	0.83	0.61
		E (kJ/mol)	3.64	3.38	3.02
MS.C	Langmuir model	Q_{max}(mg/g)	391.03	348.36	268.67
		b (L/mg)	0.0017	0.0016	0.0015
		R^2	0.96	0.96	0.93
		X^2	1.87	1.82	2.48
	Freundlich model	$1/n$	0.66	0.68	0.69
		k_F(mg/g)	2.85	2.22	1.54
		R^2	0.92	0.92	0.89
		X^2	3.77	3.47	4.07
	D-R model	β (mol^2/KJ^2)	0.0671	0.0724	0.0766
		Q_m(mg/g)	196.35	170.28	132.25
		R^2	0.95	0.95	0.97
		X^2	2.58	2.31	0.98
		E (kJ/mol)	2.73	2.63	2.55
SS.C	Langmuir model	Q_{max}(mg/g)	454.34	345.9	291.47
		b(L/mg)	0.0020	0.0023	0.0019
		R^2	0.97	0.96	0.94
		X^2	1.46	1.34	2.16
	Freundlich model	$1/n$	0.62	0.59	0.65
		k_F(mg/g)	4.64	4.56	2.46
		R^2	0.93	0.92	0.90
		X^2	3.48	3.24	3.9
	D-R model	β (mol^2/KJ^2)	0.0578	0.0549	0.06653
		Q_m(mg/g)	240.6	196.5	155.11
		R^2	0.91	0.94	0.97
		X^2	4.6	2.54	1.07
		E (kJ/mol)	2.94	3.01	2.74

with dissolving the dye molecules at high concentrations in the reaction system.[3] The proportionate relation between the starting MG concentrations and its adsorbed quantities by N.C, MS.C, and SS.C were observed clearly up to specific concentrations of 500, 600, and 600 mg/L using N.C (Figure 6A), MS.C (Figure 6B), and SS.C (Figure 6C), respectively. These MG concentrations are the equilibration concentrations at which the N.C, MS.C, and SS.C products were saturated by the adsorbed molecules of the dye and realized their actual or experimental maximum capacities. The detected best MG uptake capacities by N.C are 112.3 mg/g (293 K), 98.2 mg/g (303 K), and 78.8 mg/g (313 K) (Figure 6A). For MS.C, the measured MG capacities are 203.1 mg/g (293 K), 174.6 mg/g (303 K), and 131.4 mg/g (313 K) (Figure 6B) while the detected values by SS.C are 254.5 mg/g (293 K), 204 mg/g (303 K), and 156.7 mg/g (313 K) (Figure 6C). The detectable decrease in the N.C, MS.C, and SS.C adsorption efficiencies for MG dye with the tested values of temperature reveals the exothermic properties of their MG adsorption systems.

2.2.3.2. Classic Isotherm Models. The classic isotherm studies of MG adsorption by N.C, MS.C, and SS.C were accomplished based on the nonlinear fitting of the results with the theoretical hypotheses of Langmuir (L-G) (Figure 6, parts D−F), Freundlich (F-R) (Figure 6, parts G−I), and Dubinin−Radushkevich (D-R) (Figure 6, parts J−L) as traditional equilibrium models. The fitting parameters of R^2, as well as χ^2, revealed the adsorption of MG by the N.C, MS.C, and SS.C particles according to the traditional equilibrium hypothesis of Langmuir isotherm as compared to the hypothesis of the Freundlich Isotherm (Table 3). Considering this equilibrium behavior, the adsorbed MG molecules characterizes by homogeneous and monolayer properties on the surfaces of the N.C, MS.C, and SS.C particles.[16] Based on the estimated parameters of the Langmuir model, the theoretical maximum capacities of N.C, MS.C, and SS.C as adsorbents for MG at the best temperature value (293 K) are 153.3, 391.3, and 454.3 mg/g, respectively (Table 3). The Gaussian energies of the N.C, MS.C, and SS.C adsorption systems for MG dye were

https://doi.org/10.1021/acsomega.2c04985
ACS Omega 2022, 7, 36697−36711

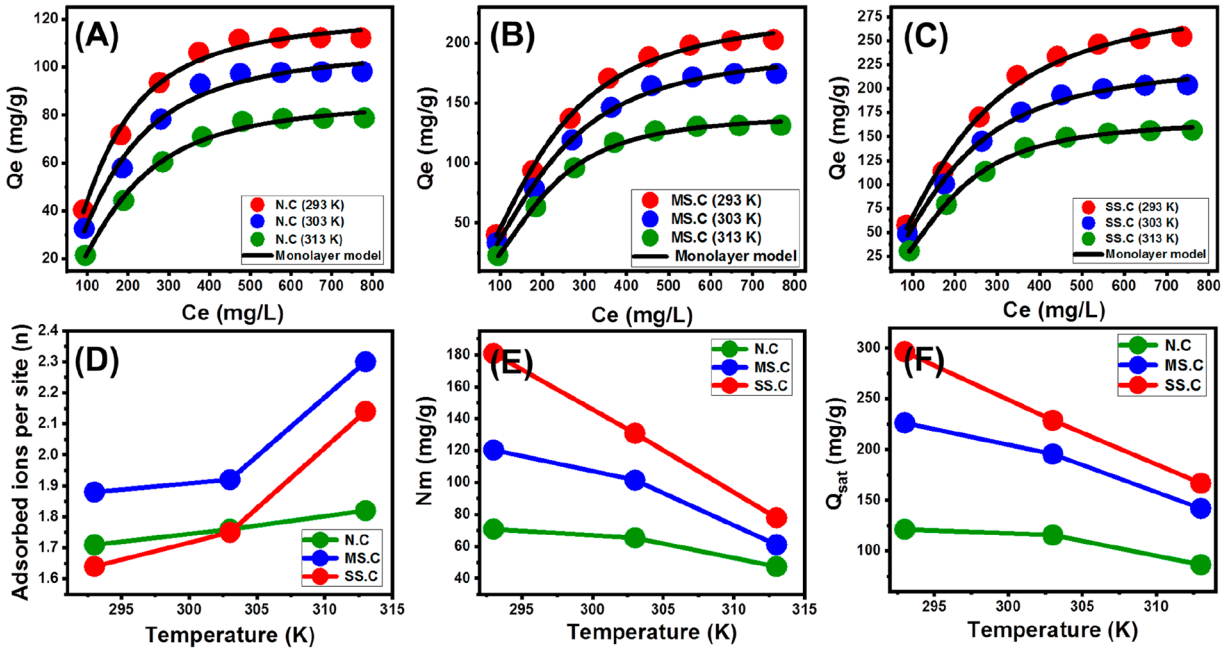

Figure 7. Fitting of the MG adsorption results with Monolayer model of one energy site (A−C), the change in the number of adsorbed ions per site with temperature (D), the change in the active sites density with temperature (E), and the change in the saturation adsorption capacities with temperature (F) (pH 9 (pH of the solutions), 0.25 g/L (coal dosage), 780 min (contact time), and 200 mL (volume)).

recognized as parameters for the addressed D-R isotherm model (Table 3). The obtained energies for N.C (3.02 to 3.6 kJ/mol), MS.C (2.55 to 2.73 kJ/mol), and SS.C (2.7 to 3.01 kJ/mol) authorize dominant effect for the physisorption mechanisms (<8 kJ/mol) during their adsorption reactions for MG molecules.[45]

2.2.3.3. Advanced Isotherm Models. Recently, statistical physics theory was applied to develop advanced isotherm models of more significance about the nature and mechanisms of the adsorption reactions. The adsorption properties of N.C, MS.C, and SS.C particles during the MG uptake reactions were evaluated and discussed considering the theoretical hypothesis of the Monolayer model with one energy site in addition to the obtained mathematical parameters either the steric parameters (number of adsorbed MG molecules per site (n), the receptor sites density (N_m), and saturation adsorption capacity of the coal products (Q_{sat})) or the energetic parameters (internal energy (E_{int}), adsorption energy (ΔE), free enthalpy (G), and entropy (S_a)) (Figure 7A−C; Table 4).

Table 4. Estimated Mathematical Parameters for the Fitting Process with a Monolayer Model of One Energy

	steric and energetic parameters					
	temp (K)	n	N_m (mg/g)	Q_{sat} (mg/g)	$C_{1/2}$ (mg/L)	ΔE (kJ/mol)
N.C	293	1.71	70.84	121.3	137.57	−3.01
	303	1.76	65.35	115.6	157.72	−3.45
	313	1.82	47.36	86.43	176.74	−3.86
MS.C	293	1.88	120.38	226.3	227.33	−4.23
	303	1.92	101.52	195.52	212.7	−4.21
	313	2.3	61.07	141.9	195.61	−4.13
SS.C	293	1.64	180.74	296.4	212.68	−4.07
	303	1.75	130.79	228.88	191.04	−3.94
	313	2.14	77.93	166.77	186.76	−4.01

2.2.3.3.1. Steric Parameters. 2.2.3.3.1.1. Number of Adsorbed MG Molecules per Site (n). The numbers of adsorbed MG molecules per each active receptor on the surfaces of N.C, MS.C, and SS.C particles can validate the orientation of the dyes on their surfaces as well as the affected mechanisms. The number of adsorbed MG molecules per each site on the surfaces of N.C (n = 1.71−1.82), MS.C (n = 1.88−2.3), and SS.C (n = 1.64−2.14) are higher than 1 (Figure 7D; Table 4). This signifies the uptake of MG on the surfaces of the coal products in nonparallel and/or vertical orientation by multimolecular mechanisms.[46,47] Moreover, the previous values validate the suitability of the active sites on the surfaces of MS.C and SS.C to adsorb up to three molecules of MG as compared to two molecules by the active sites of N.C. The remarkable increase in the number of MG molecules that were adsorbed by the active sites of N.C, MS.C, and SS.C demonstrates a considerable increase in the aggregation behaviors of the dye molecules (Figure 7D).[47−49]

2.2.3.3.1.2. Density of the Receptor Sites (N_m). The density of the receptor sites (N_m) on the surfaces of N.C, MS.C, and SS.C particles reflects strongly the quantities of the present free active sites which can be occupied by the adsorbed MG molecules (Figure 7E; Table 4). The receptor density values (N_m) during the MG adsorption by N.C are 70.84 mg/g (293 K), 65.35 mg/g (303 K), and 47.36 mg/g (313 K) and the estimated values of MS.C are 120.38 mg/g (293 K), 101.5 mg/g (303 K), and 61.01 mg/g (313 K). For SS.C, the determined values are 180.74 mg/g (293 K), 130.79 mg/g (303 K), and 77.93 mg/g (313 K). The estimated N_m parameter of SS.C and MS.C show higher values than N.C, and the values of SS.C are higher than MS.C. This demonstrates the effect of the sulfonation modification reactions in inducing the formation or activation of more active adsorption sites on the surface of the coal, which induces its adsorption capacity. Additionally, the results validate the higher effect of the sonication waves in inducing the oxidation and sulfonation efficiency of the coal

https://doi.org/10.1021/acsomega.2c04985
ACS Omega 2022, 7, 36697−36711

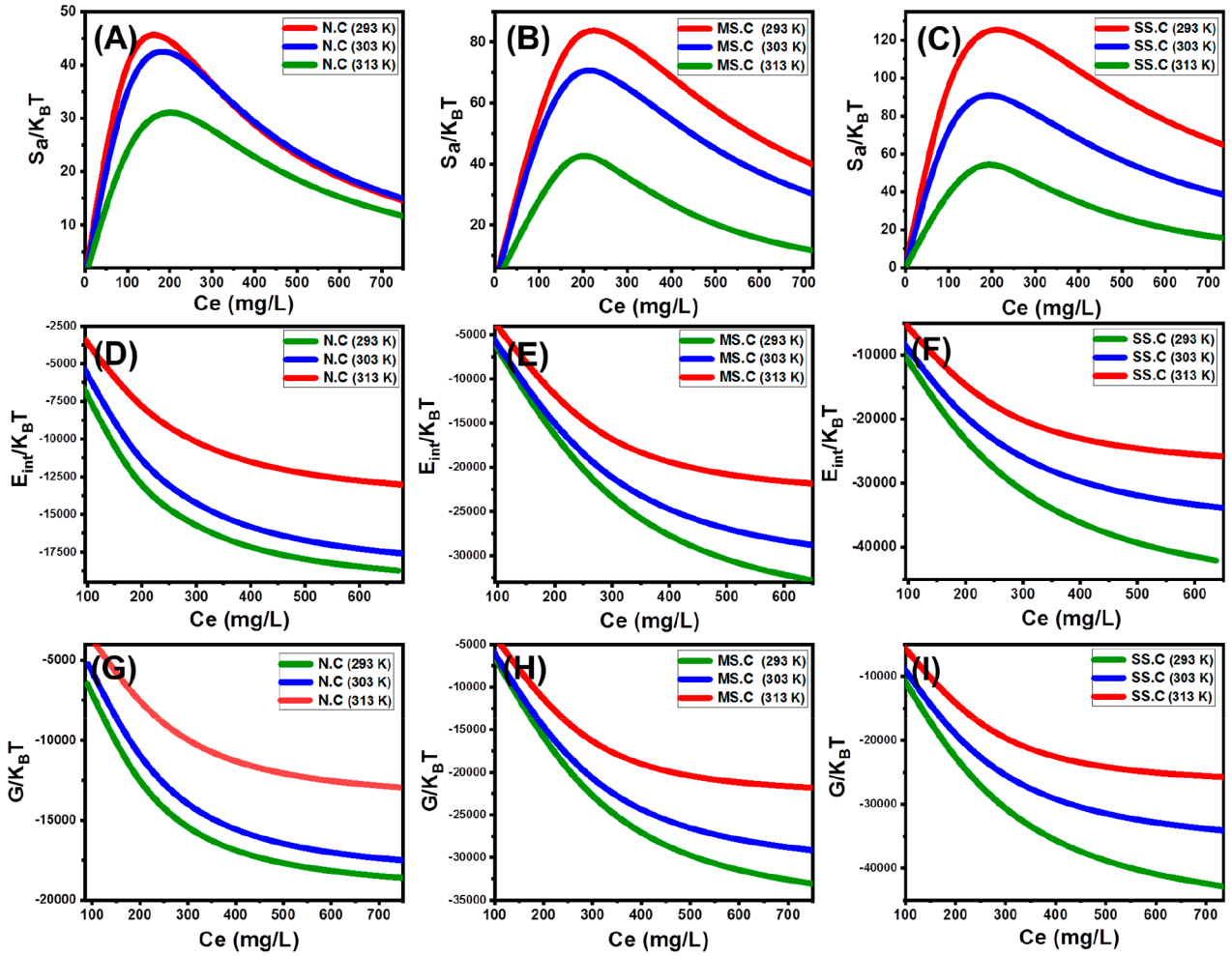

Figure 8. Change in the entropy properties with temperature and the tested concentrations (A−C), the change in the internal energy properties with temperature and the tested concentrations (D−F), and the change in the free enthalpy properties with temperature and the tested concentrations (G−I) (pH 9 (pH of the solutions), 0.25 g/L (coal dosage), 780 min (contact time), and 200 mL (volume)).

components which is in agreement with the FT-IR and chemical analysis findings in addition to its effect on enhancing the surface area and the porosity properties. Therefore, the sulfonation activation of coal by the sonication waves induces the adsorption properties of coal by enhancing the quantities and exposures of the active adsorption sites. Moreover, the observable decrease in the N_m values of N.C, MS.C, and SS.C with the adsorption temperature is in significant agreement with the estimated values of the n parameter (Figure 7E; Table 4). The increase in the aggregation efficiencies of the MG molecules during their adsorption by N.C, MS.C, and SS.C is associated with declination in the quantities of the occupied active sites.[47]

2.2.3.3.1.3. The Adsorption Capacities at the Saturation State of Q_{sat}. The adsorption capacities of N.C, MS.C, and SS.C as adsorbents for MG dye at the saturation states of their incorporated particles (Q_{sat}) are the most appropriate values that represent their maximum adsorption capacities as compared to the recognized findings of the classic isotherm models (Figure 7F; Table 4). The values of Q_{sat} depend essentially on the density of the active sites (N_m) and/or the number of adsorbed MG molecules per each site on the surfaces of N.C, MS.C, and SS.C. The attained Q_{sat} values of N.C are 121.3 mg/g (293 K), 115.6 mg/g (303 K), and 86.43 mg/g (313 K) while the calculated values of MS.C are 226.3 mg/g (293 K), 195.5 mg/g (303 K), and 141.9 mg/g (313 K) (Figure 7F; Table 4). The Q_{sat} of SS.C during the uptake of MG are 296.4 mg/g (293 K), 228.8 mg/g (303 K), and 166.7 mg/g (313 K) (Figure 7F; Table 4). This agreement between the detected Q_{sat} values and the estimated N_m values as a function of the adsorption temperature as compared to the n parameter validates the controlling role of the active sites densities on the adsorption efficiencies of the MG dye by N.C, MS.C, and SS.C. Also this explains the reported higher actual uptake capacities of the sulfonated products as compared to the raw sample especially the sulfonated sample in the presence of the sonication waves (SS.C).

2.2.3.3.2. Energetic Properties. 2.2.3.3.2.1. Adsorption Energy. The adsorption energies (ΔE) of N.C, MS.C, and SS.C as adsorption systems during the MG uptake reactions are of remarkable significance to the affecting mechanisms. The ΔE values for the MG adsorption by the coal products were determined directly from eq 1 using the values of the obtained steric parameters where $C_{1/2}$ is the concentration of MG at the half-saturation, S is the solubility of MG dye, R is the gas constant, and T is the adsorption temperature.[47]

https://doi.org/10.1021/acsomega.2c04985
ACS Omega 2022, 7, 36697−36711

$$\Delta E = RT \ln\left(\frac{S}{C_{1/2}}\right) \quad (1)$$

The adsorption systems that are characterized by adsorption energies less than 40 kJ/mol display a dominant effect for the physisorption mechanisms while the adsorption systems that exhibit energies beyond 80 kJ/mol display strong chemisorption mechanisms. The physisorption mechanisms involved different subclasses of different energy ranges such as van der Waals forces (4−10 kJ/mol), dipole bonding forces (2−29 kJ/mol), hydrophobic bonding (5 kJ/mol), coordination exchange (40 kJ/mol), and hydrogen bonding (<30 kJ/mol).[47,50] The determined MG adsorption energies using N.C (−3.01 to −3.86 kJ/mol), MS.C (−4.13 to −4.23 kJ/mol), and SS.C (−3.94 kJ/mol to −4.07 kJ/mol) are within the identified range of the physisorption mechanisms (Table 4). These signify the significant effects of the van der Waals forces in addition to the dipole bonding forces and hydrogen bonding as the operating mechanisms during the MG adsorption processes by N.C, MS.C, and SS.C.[51] The negative signs of the estimated ΔE values during the MG adsorption by N.C, MS.C, and SS.C suggest the exothermic behaviors of these reactions.

2.2.3.3.2.2. Thermodynamic Functions. 2.2.3.3.2.2.1. Entropy. The MG adsorption entropy (S_a) by N.C, MS.C, and SS.C considering the temperature of the tests as well as the concentrations of MG can signify the surficial properties of the coal particles (order and disorder). The S_a values of the MG adsorption by N.C, MS.C, and SS.C were calculated according to eq 2 using the values of the previously estimated steric parameters.[51]

$$\frac{S_a}{K_B} = N_m\left\{\ln\left(1 + \left(\frac{C}{C_{1/2}}\right)^n\right) - n\left(\frac{C}{C_{1/2}}\right)^n \frac{\ln\left(\frac{C}{C_{1/2}}\right)}{1 + \left(\frac{C}{C_{1/2}}\right)^n}\right\} \quad (2)$$

The estimated S_a values of the MG adsorption by N.C, MS.C, and SS.C exhibit reversible trends with the equilibrium concentrations of the dye without any impact of the temperature on these behaviors (Figure 8A−C). Consequently, there is an observable enhancement in the disorder properties of the N.C, MS.C, and SS.C surfaces during the MG uptake reaction at low concentrations of its molecules in the systems. Moreover, these behaviors demonstrate strong docking of the MG molecules on the distributed adsorption sites on the surfaces of N.C, MS.C, and SS.C by conducting the experiments at low dye concentrations.[47,48] The equilibrium MG concentrations that are corresponding to the maximum S_a values of the N.C adsorption system are 182.05 mg/L (293 K), 185.52 mg/L (303 K), and 188.9 mg/L (313 K) (Figure 8A). For the MS.C system, the identified concentrations are 176.6 mg/L (293 K), 180.3 mg/L (303 K), and 184.15 mg/L (313 K) (Figure 8B). Regarding the MG uptake system by SS.C, the identified concentrations are 171.6 mg/L (293 K), 174.8 mg/g (303 K), and 180.15 mg/g (313 K) (Figure 8C). These MG equilibration concentrations exhibit values close to estimated values of the dye concentrations during the half-saturation states of N.C, MS.C, and SS.C adsorbents. Consequently, the previously reported MG concentrations reflect mostly the complete occupation of the distributed active sites on the surfaces of N.C, MS.C, and SS.C with the MG molecules, and in turn, no further dye can be docked. The observed sharp dropping in the values of S_a of the N.C, MS.C, and SS.C adsorption systems for MG dye beyond the previously reported equilibrium concentrations is associated with a decrease in the adsorption sites' availability and freedom degrees in addition to the diffusions of the dye molecules.[46]

2.2.3.3.2.2.2. Internal Energy and Free Enthalpy. The internal energy (E_{int}) as a thermodynamic function of the MG adsorption by N.C, MS.C, and SS.C were estimated utilizing eq 3 which depends mainly on the translation partition (Z_v) and the values of other steric parameters.[51]

$$\frac{E_{int}}{K_B T} = nN_m\left[\left(\frac{\left(\frac{C}{C_{1/2}}\right)^n \ln\left(\frac{C}{Z_v}\right)}{1 + \left(\frac{C}{C_{1/2}}\right)^n}\right) - \left(\frac{n \ln\left(\frac{C}{C_{1/2}}\right)\left(\frac{C}{C_{1/2}}\right)^n}{1 + \left(\frac{C}{C_{1/2}}\right)^n}\right)\right] \quad (3)$$

The E_{int} values of the N.C, MS.C, and SS.C adsorption systems for MG exhibit negative signs either at the different values of the dye concentrations or the tested temperature values which signify the spontaneous properties of these processes (Figure 8D−F). Moreover, the decrease in these values for the tests which were conducted under high-temperature conditions demonstrates the exothermic properties of the MG adsorption by N.C, MS.C, and SS.C (Figure 8D−F). Moreover, the negative signs of the free enthalpy (G) (eq 4) considering the corresponding MG concentrations and the temperature of the tests confirm the spontaneous and exothermic properties of the MG adsorption by N.C, MS.C, and SS.C (Figure 8G−I).

$$\frac{G}{K_B T} = nN_m \frac{\ln\left(\frac{C}{Z_v}\right)}{1 + \left(\frac{C_{1/2}}{C}\right)^n} \quad (4)$$

2.2.4. Recyclability. The recyclability of N.C, MS.C, and SS.C as adsorbents for MG dye was studied as essential factors during the assessment of the products for commercial and realistic scale applications. The spent particles of N.C, MS.C, and SS.C were washed strongly, utilizing distilled water for 10 min, and this was repeated for five cycles. After that, the washed N.C, MS.C, and SS.C were dried at 60 °C for 8 h to be reused again in other MG adsorption cycles. The conducted recyclability tests of the coal adsorbents for MG were performed considering the adsorption variables at pH 9 (pH of the solutions), 0.25 g/L (coal dosage), 780 min (contact time), 200 mL (volume), 100 mg/L (MG concentration), and 293 K (temperature). The determined MG adsorption efficiencies using N.C as well as MS.C and SS.C adsorbents reflect significant stability and remarkable recyclability values of the products of the modified coal considering the three investigated recyclability runs (Figure 9). The recyclability of N.C in the five MG uptake cycles resulted in adsorption efficiencies of 71.9 mg/g (cycle 1), 71 mg/g (cycle 2), 66.3 mg/g% (cycle 3), 61.2 mg/g (cycle 4), and 54.7 mg/g (cycle 5) (Figure 9). For the recyclability of MS.C, the adsorbed quantities are 93.8 mg/g (cycle 1), 93 mg/g (cycle 2), 90.2 mg/g% (cycle 3), 85.6 mg/g (cycle 4), and 78.4 mg/g (cycle 5) (Figure 9). For SS.C, its determined capacities of MG are 113.3 mg/g (cycle 1), 113 mg/g (cycle 2), 111.4 mg/g% (cycle 3), 107.2 mg/g (cycle 4), and 101.4 mg/g (cycle 5). There are

https://doi.org/10.1021/acsomega.2c04985
ACS Omega 2022, 7, 36697−36711

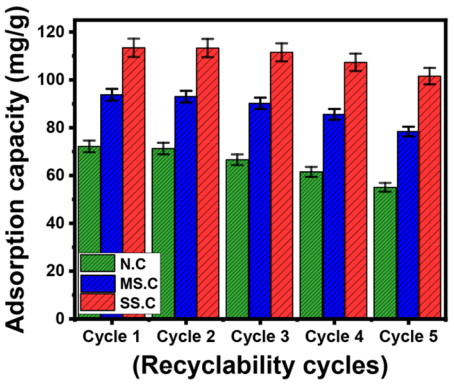

Figure 9. Recyclability properties of N.C, MS.C, and SS.C during the adsorption of MG dye pH 9 (pH of the solutions), 0.25 g/L (coal dosage), 780 min (contact time), 200 mL (volume), 100 mg/L (MG concentration), and 293 K (temperature)).

small declinations in determined MG adsorption efficiencies of N.C, MS.C, and SS.C within the regular repeating of the recyclability cycles. This might be assigned to the predicted leaching of the coal components during the washing processes and/or the continuous formation of chemical complexes between the MG molecules and the chemical structures of the coal components.

2.2.5. The Formation and Operation Mechanism of Sulfonated Coal. The sulfonation of coal as a heterogeneous organic structure of different organic components including cellulose, lignin, and resin is controlled by the availability of effective electrophilic species. Such species are the main components in the systems that can functionalize and affect chemically the aromatic components of coal.[52] The interaction between the chemical activator (H_2SO_4) and the organic structure of coal resulted in significant grabbing of the hydrogen ions by the −OH groups of the incorporated acid molecules. This in turn causes remarkable destruction of the present oxygen−hydrogen bond and the formation of H_2O molecules (Figure 10).[26] During this reaction, another interaction occurs between the protonated oxygen and lone pair electrons resulting in a new π bond with the incorporated sulfur ions creating protonated trioxide.[26] The sulfur ions and the formed sulfur trioxide exhibit significant electronegativity therefore it acts as effective electrophiles during the performed sulfonation reactions.[25] Consequently, the sulfur ions attack the structural benzene rings which are of destructive effects on the double bonds of the aromatic rings which in turn induce the entrapping of the S-bearing chemical groups ($-SO_3H$) (Figure 10). At the same time, the interaction between the H_2SO_4 acid resulted in HSO_4^- radicals which act as base centers for effective removal of the hydrogen protons.[52] Moreover, the progressive oxidation of the coal structure with the sulfuric acid causes a significant transformation of the present −OH groups into active carboxyl groups (COOH). Therefore, the sulfonated coal structure becomes enriched in $COOH^-$, OH^-, and $-SO_3H$ groups which are very active sites during the adsorption reactions especially the cationic ions or molecules (Figure 10).

The sonication waves during the sulfonation process induce strongly the efficiency of the reaction and the entrapment of the acidic groups. This was assigned to the impact of the sonication waves in inducing mixing properties and the homogeneity between the different reactants and in turn the interaction between the acid molecules and the coal fractions.[53,54] This is credited to the cavitation phenomenon which is associated with the sonication waves that involve the formation of fine acid droplets or bubbles along the interface between the acid and the coals particles.[53,54] The sudden collapse of these droplets creates additional pressure centers, microjets, shockwaves, and microstreams, which induce the mixing and interaction efficiency.[55] Moreover, the presence of the sonication waves induces the disintegration of the present coal components into finer particles of enhanced surface area.[56]

Considering the present functional chemical groups and the previous findings of the adsorption mechanism based on the adsorption energy and Gaussian energy, the uptake of MG dye by the sulfonated coal products might be involved three mechanisms (Figure 10). The first mechanism involved the electrostatic attraction between the positively charged MG dye molecules and the negatively charged groups of coal. The second mechanism involved the formation of hydrogen bonds between the free hydrogen of the sulfonated coal surfaces and the nitrogen atoms of the MG dye chemical structure. The third mechanism involved $\pi-\pi$ interactions between the π-electron system of the sulfonated coal and the aromatic rings of

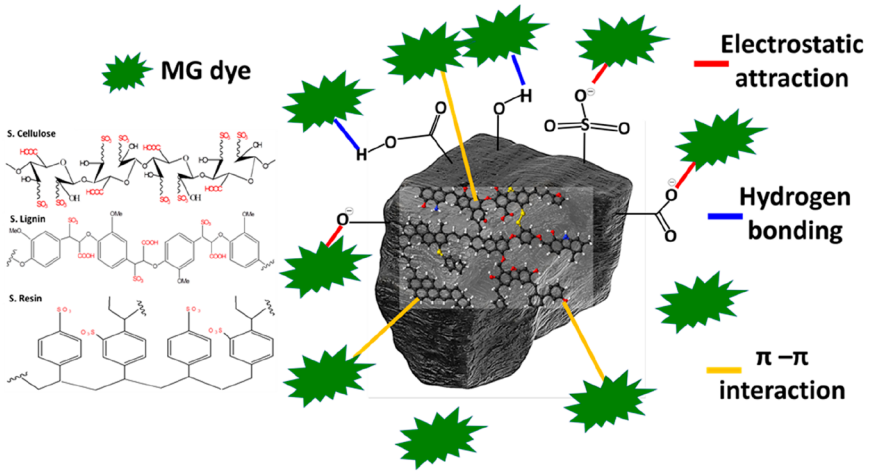

Figure 10. Schematic diagram for the adsorption mechanism of MG dye by the sulfonated coal samples.

https://doi.org/10.1021/acsomega.2c04985
ACS Omega 2022, 7, 36697−36711

MG molecules involving a combination of dispersion and dipole−induced dipole interactions (Figure 10).

2.2.6. Comparison Study. The estimated capacities of sulfonated coal adsorbents were compared with other studied adsorbents in the literature (Table 5). The present results demonstrate the higher capacities of the sulfonated coal products (MS.C and SS.C) as compared to the presented materials including graphene oxide/Fe_3O_4 composite, modified CNTs, Fe-Fe_2O_3@PDA, ZnO-NRs-AC, and halloysite nanotubes (Table 5). This validates the value of the prepared sulfonation oxidation of coal especially using the sonication waves in developing enhanced adsorbents of high adsorption capacities, facile synthesis procedures, significant recyclability, low cost, and available precursors.

Table 5. Comparison between the Studied Coal-Based Adsorbents and Other Studied Adsorbents in Literature

adsorbents	Q_{max}(mg/g)	references
Fe−Fe_2O_3@PDA	61.22	57
ZnO-NRs-AC	59.17	58
aerobic granules	56.8	59
organoclay	40.4	60
Halloysite nanotubes	99.6	61
modified carbon nano tubes	172	62
Limonia acidizsima	35.48	63
iron humate	19.2	64
graphene oxide/Fe_3O_4	179	65
N.C (Q_{sat})	121.3	this study
N.C (Q_{max})	153.37	this study
MS.C (Q_{sat})	226.3	this study
MS.C (Q_{max})	391.03	this study
SS.C (Q_{sat})	296.4	this study
SS.C (Q_{max})	454.34	this study

3. CONCLUSION

Natural coal (N.C) was treated with H_2SO_4 by normal stirring and by the sonication waves producing modified products of enhanced adsorption capacity for malachite green dye. The sulfonation processes enhanced the surface area (MS.C (27.2 m^2/g) and SS.C (45.8 m^2/g)) and functionalized the coal surface by SO_3−H and other active oxygenated chemical groups. The sulfonation by sonication waves (SS.C) resulted in higher surface area and functionalization efficiencies as compared to normal stirring sulfonation (MS.C) considering the acid density value (14.2 mmol/g) and sulfur content (13.2 wt. %). The sulfonation modification induces the adsorption of MG dye by N.C (121.3 mg/g) to 226.3 and 296.4 mg/g by MS.C and SS.C, respectively. This was assigned to the increase in the quantities of the active sites which are 180.7 and 120.38 mg/g for SS.C and MS.C as compared to 70.8 mg/g for N.C. This validates the significant effect of the sonication process in inducing the adsorption activity of coal in addition to the applied sonication techniques. The uptake of MG occurred by exothermic, spontaneous, and physisorption mechanisms involving van der Waals forces, hydrogen bonds, and dipole bonding forces considering the adsorption energy (<40 kJ/mol) and thermodynamic functions.

4. METHODOLOGY

4.1. Materials. The coal sample which was used in the sulfonation processes is a sub-bituminous coal sample used in sulfonation processes obtained from the El-Maghara mine, the Sinai peninsula, Egypt. The chemical composition was determined based on the proximate and ultimate analyses (Table S1). The investigated malachite green dye ($C_{23}H_{26}N_2O,CI_{42}$) was estimated from Sigma-Aldrich; Egypt.

4.2. Sulfonation Processes. The sample was prepared based on the reported procedures by 19 (Figure S1). The raw sample was ground using a home blender to be within the size range from 20 up to 70 μm. The ground product (10 g) was mixed with sulfuric acid (95%) within two beakers, and each beaker contains 100 mL of the acid as separated systems. The homogenization process of the first system was continued for 90 min by the normal magnetic stirring process at a fixed speed of 500 rpm and an adjusted temperature of 150 °C. The homogenization of the second system (beaker) was accomplished in the presence of a sonication source (240 W) at an adjusted temperature of 150 min for 60 min. After each test, the obtained samples were washed and neutralized with distilled water for three runs, and each run consumed 10 min. This was followed by gentle drying of the samples using a digital dryer for 10 h at 65 °C. Finally, the products were collected, preserved in specific containers, and labeled as MS.C (sulfonation by magnetic stirring) and SS.C (sulfonation by sonication waves).

4.3. Analytical Techniques. The impact of the sulfonation conditions was assessed considering the changes in the structural, textural, chemical, and morphological properties. The structure of the modified samples was studied based on their XRD patterns utilizing an X-ray diffractometer (PANalytical (Empyrean)). The incorporated sulfonic groups and the impact of the acid oxidation reactions were followed based on the FT-IR spectra of the produced structures using a Fourier transform infrared spectrometer (FTIR−8400S). The morphological features of the modified coals as compared to the raw sample were studied considering the SEM images of the samples using a scanning electron microscope (Gemini, Zeiss-Ultra 55)). The impact of the sulfonation processes on the surface area was followed considering the BET surface area of the samples using the Beckman Coulter surface area analyzer (SA3100 type). The ζ-potential values were measured using Zetasizer attached to the ζ-cell (Malvern, version 7.11) at different pH, and the results were applied to determine the pH value at zero point charge ($pH_{(ZPC)}$).

4.4. Adsorption Studies. The adsorption of the selected synthetic dye (malachite green (MG) (Figure S2) by normal raw coals (N.C), sulfonated coals by normal stirring (MS.C), and sulfonated coal by sonication waves (SS.C) were performed as batch tests considering the main experimental variables such as pH (2 until 9), contact time (30−960 min), and dye concentration (100−800 mg/L) at a fixed volume of 200 mL, considering the change in the temperature of the equilibrium experiments from 293 K up to 313 K. The tests were conducted in triplicate forms considering the average values for all the inserted results. The rest dye concentrations after each test were determined using a UV−vis spectrophotometer considering the value of λ max of the MG dye and the adsorption capacity (Q_e) was calculated from eq 5.

$$Q_e\ (\mathrm{mg/g}) = \frac{(C_o - C_e)V}{m} \tag{5}$$

The nonlinear fitting degrees with the addressed classic kinetic and isotherm models (Table S2) were considered based on the correlation coefficient (R^2) (eq 6) and chi-squared (χ^2)

https://doi.org/10.1021/acsomega.2c04985
ACS Omega 2022, 7, 36697−36711

value (eq 7). However, the fitting degrees with the evaluated advanced isotherm models based on the statistical physics theory (Table S2) were estimated based on the correlation coefficient (R^2) and root-mean-square error, (RMSE) (eq 8) where the used symbols of m', p, $Q_{i_{cal}}$, and $Q_{i_{exp}}$ refer to the inserted data, the experimental variables, adsorbed quantities of MG, and actual adsorbed quantities of the MG molecules, respectively.

$$R^2 = 1 - \frac{\sum (Q_{e,\exp} - Q_{e,\mathrm{cal}})^2}{\sum (Q_{e,\exp} - Q_{e,mean})^2} \quad (6)$$

$$\chi^2 = \sum \frac{(Q_{e,\exp} - Q_{e,\mathrm{cal}})^2}{Q_{e,\mathrm{cal}}} \quad (7)$$

$$\mathrm{RMSE} = \sqrt{\frac{\sum_{i=1}^{m} (Q_{i_{cal}} - Q_{i_{exp}})^2}{m' - p}} \quad (8)$$

■ ASSOCIATED CONTENT

Supporting Information

The Supporting Information is available free of charge at https://pubs.acs.org/doi/10.1021/acsomega.2c04985.

Proximate and ultimate analysis of the original coal sample (Table S1) in addition to the representative equations of the kinetic and isotherm models (Table S2) and a schematic diagram of the of the sulfonation processes (Figure S1) and the molecular structure of malachite green dye (Figure S2) (PDF)

■ AUTHOR INFORMATION

Corresponding Author

Mostafa R. Abukhadra − *Geology Department, Faculty of Science, Beni-Suef University, Beni-Suef 65211, Egypt; Materials Technologies and their Applications Lab, Geology Department, Faculty of Science, Beni-Suef University, Beni-Suef City 65211, Egypt;* orcid.org/0000-0001-5404-7996; Phone: +2001288447189; Email: Abukhadra89@Science.bsu.edu.eg

Authors

Ali A. AlHammadi − *Chemical Engineering Department, Khalifa University of Science and Technology, Abu Dhabi, United Arab Emirates; Center for Catalysis and Separation (CeCas), Khalifa University of Science and Technology, Abu Dhabi, United Arab Emirates;* orcid.org/0000-0002-2747-2492

Rania Nasser − *Matrail Sciences and Nanotechnology Department, Faculty of Post Graduate Studies for Advanced Sciences, Beni-Suef University, Beni-Suef City 65211, Egypt*

Mohamed S. Shaban − *Geology Department, Faculty of Science, New Valley University, Kharga, New Valley Governorate 1064188, Egypt;* orcid.org/0000-0002-4368-8269

Sarah I. Othman − *Biology Department, Faculty of Science, Princess Nourah bint Abdulrahman University, Riyadh 11564, Saudi Arabia*

Jong Seong Khim − *School of Earth & Environmental Sciences, College of Natural Sciences, Seoul National University, Seoul 08826, Republic of Korea;* orcid.org/0000-0001-7977-0929

Jamaan S. Ajarem − *Zoology Department, College of Science, King Saud University, Riyadh 11451, Saudi Arabia*

Ahmed A. Allam − *Zoology Department, Faculty of Science, Beni-Suef University, Beni-Suef 65211, Egypt*

Complete contact information is available at: https://pubs.acs.org/10.1021/acsomega.2c04985

Author Contributions

This article was written through the contributions of all authors. All authors have given approval to the final version of the manuscript

Notes

The authors declare no competing financial interest.

Recommendation. Further studies will be conducted to evaluate the efficiency of the coals based adsorbents in realistic removal of malachite green dye from real industrial wastewater based on continuous fixed bed column studies considering the competitive ions, the real pH of the water, the lifetime of the coal bed, and the adsorption capacity and regeneration properties of the bed.

■ ACKNOWLEDGMENTS

The authors acknowledge Researchers Supporting Project Number RSP-2021/149, King Saud University, Riyadh, Saudi Arabia. Also, the authors acknowledge Princess Nourah bint Abdulrahman University Researchers Supporting Project Number PNURSP2022R5, Princess Nourah bint Abdulrahman University, Riyadh, Saudi Arabia

■ REFERENCES

(1) Sajid, M.; Sajid Jillani, S. M.; Baig, N.; Alhooshani, K. Layered double hydroxide-modified membranes for water treatment: Recent advances and prospects. *Chemosphere* **2022**, *287*, 132140.

(2) Yang, X.; Wang, J.; El-Sherbeeny, A. M.; AlHammadi, A. A.; Park, W. H.; Abukhadra, M. R. Insight into the adsorption and oxidation activity of a ZnO/piezoelectric quartz core-shell for enhanced decontamination of ibuprofen: Steric, energetic, and oxidation studies. *Chem. Eng. J.* **2022**, *431*, 134312.

(3) Salam, M. A.; Abukhadra, M. R.; Mostafa, M. Effective decontamination of As (V), Hg (II), and U (VI) toxic ions from water using novel muscovite/zeolite aluminosilicate composite: adsorption behavior and mechanism. *Environ. Sci. Pollut. Res.* **2020**, *27*, 13247−13260.

(4) Song, Y.; Tan, J.; Wang, G.; Zhou, L. Superior amine-rich gel adsorbent from peach gum polysaccharide for highly efficient removal of anionic dyes. *Carbohydr. Polym.* **2018**, *199*, 178−185.

(5) Li, C.; Wang, X.; Meng, D.; Zhou, L. Facile synthesis of low-cost magnetic biosorbent from peach gum polysaccharide for selective and efficient removal of cationic dyes. *Int. J. Biol. Macromol.* **2018**, *107*, 1871−1878.

(6) Kakavandi, B.; Takdastan, A.; Pourfadakari, S.; Ahmadmoazzam, M.; Jorfi, S. Heterogeneous catalytic degradation of organic compounds using nanoscale zero-valent iron supported on kaolinite: Mechanism, kinetic and feasibility studies. *J. Taiwan Inst Chem. Eng.* **2019**, *96*, 329−340.

(7) Abukhadra, M. R.; Mostafa, M.; El-Sherbeeny, A. M.; El-Meligy, M. A.; Nadeem, A. Instantaneous adsorption of synthetic dyes from an aqueous environment using kaolinite nanotubes: Equilibrium and thermodynamic studies. *ACS omega* **2021**, *6* (1), 845−856.

(8) Abukhadra, M. R.; El-Meligy, M. A.; El-Sherbeeny, A. M. Evaluation and characterization of Egyptian ferruginous kaolinite as adsorbent and heterogeneous catalyst for effective removal of safranin-O cationic dye from water. *Arab. J. Geosci.* **2020**, *13* (4), 1−13.

(9) Pathania, D.; Dhar, S.; Sharma, A.; Srivastava, A. K. Decolourization of noxious safranin-T from wastewater using Mangifera indica as precursor. *Environmental Sustainability* **2021**, *4* (2), 355−364.
(10) Mohamed, F.; Abukhadra, M. R.; Shaban, M. Removal of safranin dye from water using polypyrrole nanofiber/Zn-Fe layered double hydroxide nanocomposite (Ppy NF/Zn-Fe LDH) of enhanced adsorption and photocatalytic properties. *Sci. Total Environ.* **2018**, *640*, 352−363.
(11) Eltaweil, A. S.; Ali Mohamed, H.; Abd El-Monaem, E. M.; ElSubruiti, G. M. Mesoporous magnetic biochar composite for enhanced adsorption of malachite green dye: Characterization, adsorption kinetics, thermodynamics and isotherms. *Adv. Powder Technol.* **2020**, *31*, 1253−1263.
(12) Rabie, A. M.; Abukhadra, M. R.; Rady, A. M.; Ahmed, S. A.; Labena, A.; Mohamed, H. S.; Betiha, M. A.; Shim, J. J. Instantaneous photocatalytic degradation of malachite green dye under visible light using novel green Co−ZnO/algae composites. *Res. Chem. Intermed.* **2020**, *46* (3), 1955−1973.
(13) Saad, A. M.; Abukhadra, M. R.; Abdel-Kader Ahmed, S.; Elzanaty, A. M.; Mady, A. H.; Betiha, M. A.; Shim, J.-J.; Rabie, A. M. Photocatalytic degradation of malachite green dye using chitosan supported ZnO and Ce−ZnO nano-flowers under visible light. *J. Environ. Manage.* **2020**, *258*, 110043.
(14) Refat, M. S.; Saad, H. A.; Gobouri, A. A.; Alsawat, M.; Adam, A. M. A.; El-Megharbel, S. M. Charge transfer complexation between some transition metal ions with azo Schiff base donor as a smart precursor for synthesis of nano oxides: An adsorption efficiency for treatment of Congo red dye in wastewater. *J. Mol. Liq.* **2022**, *345*, 117140.
(15) Maruthupandy, M.; Muneeswaran, T.; Chackaravarthi, G.; Vennila, T.; Anand, M.; Cho, W.-S.; Quero, F. Synthesis of chitosan/SnO_2 nanocomposites by chemical precipitation for enhanced visible light photocatalytic degradation efficiency of congo red and rhodamine-B dye molecules. *J. Photochem. Photobiol.* **2022**, *430*, 113972.
(16) Omidinasab, M.; Rahbar, N.; Ahmadi, M.; Kakavandi, B.; Ghanbari, F.; Kyzas, G. Z.; Martinez, S. S.; Jaafarzadeh, N. Removal of vanadium and palladium ions by adsorption onto magnetic chitosan nanoparticles. *Environ. Sci. Pollut. Res.* **2018**, *25* (34), 34262−34276.
(17) Rezaei Kalantry, R.; Jonidi Jafari, A.; Esrafili, A.; Kakavandi, B.; Gholizadeh, A.; Azari, A. Optimization and evaluation of reactive dye adsorption on magnetic composite of activated carbon and iron oxide. *Desalination Water Treat.* **2016**, *57* (14), 6411−6422.
(18) Jiang, Y.; Abukhadra, M. R.; Refay, N. M.; Sharaf, M. F.; El-Meligy, M. A.; Awwad, E. M. Synthesis of chitosan/MCM-48 and β-cyclodextrin/MCM-48 composites as bio-adsorbents for environmental removal of Cd^{2+} ions; kinetic and equilibrium studies. *React. Funct. Polym.* **2020**, *154*, 104675.
(19) Abukhadra, M. R.; Soliman, S. R.; Bin Jumah, M. N.; Othman, S. I.; AlHammadi, A. A.; Alruhaimi, R. S.; Albohairy, F. M.; Allam, A. A. Insight into the sulfonation conditions on the activity of sub-bituminous coal as acidic catalyst during the transesterification of spent corn oil: effect of sonication waves. *Sustain. Chem. Pharm.* **2022**, *27*, 100691.
(20) Surip, S. N.; Abdulhameed, A. S.; Garba, Z. N.; Syed-Hassan, S. S. A.; Ismail, K.; Jawad, A. H. H_2SO_4-treated Malaysian low rank coal for methylene blue dye decolourization and cod reduction: optimization of adsorption and mechanism study. *Surf. Interfaces.* **2020**, *21*, 100641.
(21) Zeng, S.; Long, J.; Sun, J.; Wang, G.; Zhou, L. A review on peach gum polysaccharide: Hydrolysis, structure, properties and applications. *Carbohydr. Polym.* **2022**, *279*, 119015.
(22) Shaban, M.; Abukhadra, M. R.; Shahien, M. G.; Khan, A. A. P. Upgraded modified forms of bituminous coal for the removal of safranin-T dye from aqueous solution. *Environ. Sci. Pollut. Res.* **2017**, *24*, 18135−18151.
(23) Liu, Z.; Zhou, A.; Wang, G.; Zhao, X. Adsorption behavior of methyl orange onto modified ultrafine coal powder. *Chin. J. Chem. Eng.* **2009**, *17* (6), 942−948.
(24) Hassani, A.; Alidokht, L.; Khataee, A. R.; Karaca, S. Optimization of comparative removal of two structurally different basic dyes using coal as a low-cost and available adsorbent. *J. Taiwan Inst. Chem. Eng.* **2014**, *45* (4), 1597−1607.
(25) Yu, H.; Niu, S.; Bai, T.; Tang, X.; Lu, C. Microwave-assisted preparation of coal-based heterogeneous acid catalyst and its catalytic performance in esterification. *J. Clean. Prod.* **2018**, *183*, 67−76.
(26) Tang, X.; Niu, S.; Zhao, S.; Zhang, X.; Li, X.; Yu, H.; Lu, C.; Han, K. Synthesis of sulfonated catalyst from bituminous coal to catalyze esterification for biodiesel production with promoted mechanism analysis. *J. Ind. Eng. Chem.* **2019**, *77*, 432−440.
(27) Flores, K. P.; Omega, J. L. O.; Cabatingan, L. K.; Go, A. W.; Agapay, R. C.; Ju, Y. H. simultaneously carbonized and sulfonated sugarcane bagasse as solid acid catalyst for the esterification of oleic acid with methanol. *Renew. Energy.* **2019**, *130*, 510−523.
(28) Fonseca, J. M.; Spessato, L.; Cazetta, A. L.; Bedin, K. C.; Melo, S. A.; Souza, F. L.; Almeida, V. C. Optimization of sulfonation process for the development of carbon-based catalyst from crambe meal via response surface methodology. *Energy Convers. Manag.* **2020**, *217*, 112975.
(29) Kurková, M.; Klika, Z.; Kliková, C.; Havel, J. Humic acids from oxidized coals. *Chemosphere* **2004**, *54* (8), 1237−1245.
(30) Ibrahim, S. M.; El-Sherbeeny, A. M.; Shim, J. J.; AlHammadi, A. A.; Abukhadra, M. R. -SO_3H-functionalization of sub-bituminous coal as a highly active acidic catalyst during the transesterification of spent sunflower oil; characterization, application, and mechanism. *Energy Rep.* **2021**, *7*, 8699−8710.
(31) Jawad, A. H.; Mehdi, Z. S.; Mohd Ishak, M. A.; Ismail, K. Large surface area activated carbon from low-rank coal via microwave-assisted KOH activation for methylene blue adsorption. *Desalin. Water Treat* **2018**, *110*, 239−249.
(32) Zailan, Z.; Tahir, M.; Jusoh, M.; Zakaria, Z. Y. A review of sulfonic group bearing porous carbon catalyst for biodiesel production. *Renew. Energy.* **2021**, *175*, 430−452.
(33) Zhang, H.; Luo, X.; Li, X.; Chen, G. Z.; He, F.; Wu, T. Preparation and characterization of a sulfonated carbon-based solid acid microspheric material) SCSAM) and its use for the esterification of oleic acid with methanol. *Austin Chem. Eng.* **2016**, *3* (1), 1024.
(34) Farabi, M. A.; Ibrahim, M. L.; Rashid, U.; Taufiq-Yap, Y. H. Esterification of palm fatty acid distillate using sulfonated carbon-based catalyst derived from palm kernel shell and bamboo. *Energy Convers. Manag.* **2019**, *181*, 562−570.
(35) Wong, W. Y.; Lim, S.; Pang, Y. L.; Shuit, S. H.; Chen, W. H.; Lee, K. T. Synthesis of renewable heterogeneous acid catalyst from oil palm empty fruit bunch for glycerol-free biodiesel production. *Sci. Total Environ.* **2020**, *727*, 138534.
(36) Araujo, R. O.; Chaar, J. d. S.; Queiroz, L. S.; da Rocha Filho, G. N.; da Costa, C. E. F.; da Silva, G. C.; Landers, R.; Costa, M. J.; Goncalves, A. A.; de Souza, L. K. Low temperature sulfonation of acai stone biomass derived carbons as acid catalysts for esterification reactions. *Energy Convers. Manag.* **2019**, *196*, 821−830.
(37) Mateo, W.; Lei, H.; Villota, E.; Qian, M.; Zhao, Y.; Huo, E.; Zhang, Q.; Lin, X.; Wang, C. One-step synthesis of biomass-based sulfonated carbon catalyst by direct carbonization-sulfonation for organosolv delignification. *Bioresour. Technol.* **2021**, *319*, 124194.
(38) Mostafa, M.; Bin Jumah, M. N.; Othman, S. I.; Alruhaimi, R. S.; Salama, Y. F.; Allam, A. A.; Abukhadra, M. R. Effective removal of different species of organophosphorus pesticides (acephate, omthosate, and methyl parathion) using chitosan/Zeolite-A as multifunctional adsorbent. *Environ. Technol. Innov.* **2021**, *24*, 101875.
(39) Ashraf, M.-T.; AlHammadi, A. A.; El-Sherbeeny, A. M.; Alhammadi, S.; Al Zoubi, W.; Ko, Y. G.; Abukhadra, M. R. Synthesis of cellulose fibers/Zeolite-A nanocomposite as an environmental adsorbent for organic and inorganic selenium ions: Characterization and advanced equilibrium studies. *J. Mol. Liq.* **2022**, *360*, 119573.

https://doi.org/10.1021/acsomega.2c04985
ACS Omega 2022, 7, 36697−36711

(40) Fu, H.; Yang, Y.; Zhu, R.; Liu, J.; Usman, M.; Chen, Q.; He, H. Superior adsorption of phosphate by ferrihydrite-coated and lanthanum-decorated magnetite. *J. Colloid Interface Sci.* **2018**, *530*, 704−713.
(41) El-Sherbeeny, A. M.; Ibrahim, S. M.; AlHammadi, A. A.; Soliman, A. T. A.; Shim, J. J.; Abukhadra, M. R. Effective retention of radioactive Cs^{+} and Ba^{2+} ions using β-cyclodextrin functionalized diatomite (β-CD/D) as environmental adsorbent characterization, application, and safety. *Surf. Interfaces* **2021**, *26*, 101434.
(42) Huang, Y.; Li, S.; Chen, J.; Zhang, X.; Chen, Y. Adsorption of Pb (II) on mesoporous activated carbons fabricated from water hyacinth using H_3PO_4 activation: adsorption capacity, kinetic and isotherm studies. *Appl. Surf. Sci.* **2014**, *293*, 160−168.
(43) Kakavandi, B.; Raofi, A.; Peyghambarzadeh, S. M.; Ramavandi, B.; Niri, M. H.; Ahmadi, M. Efficient adsorption of cobalt on chemical modified activated carbon: characterization, optimization and modeling studies. *Desalination Water Treat.* **2018**, *111*, 310−321.
(44) Huang, M.; Tu, H.; Chen, J.; Liu, R.; Liang, Z.; Jiang, L.; Shi, X.; Du, Y.; Deng, H. Chitosan-rectorite nanospheres embedded aminated polyacrylonitrile nanofibers via shoulder-to-shoulder electrospinning and electrospraying for enhanced heavy metal removal. *Appl. Surf. Sci.* **2018**, *437*, 294−303.
(45) Abdel Salam, M.; Mokhtar, M.; Albukhari, S. M.; Baamer, D. F.; Palmisano, L.; Jaremko, M.; Abukhadra, M. R. Synthesis and Characterization of Green ZnO@ polynaniline/Bentonite Tripartite Structure (G. Zn@ PN/BE) as Adsorbent for As(V) Ions: Integration, Steric, and Energetic Properties. *Polymers* **2022**, *14* (12), 2329.
(46) Sellaoui, L.; Guedidi, H.; SarraWjihi; Reinert, L.; Knani, S.; Duclaux, L.; Ben Lamine, A. Experimental and theoretical studies of adsorption of ibuprofen on raw and two chemically modified activated carbons: new physicochemical interpretations. *RSC Adv.* **2016**, *6* (15), 12363−12373.
(47) Dhaouadi, F.; Sellaoui, L.; Badawi, M.; Reynel-Ávila, H. E.; Mendoza-Castillo, D. I.; Jaime-Leal, J. E.; Bonilla-Petriciolet, A.; Lamine, A. B. Statistical physics interpretation of the adsorption mechanism of Pb^{2+}, Cd^{2+} and Ni^{2+} on chicken feathers. *J. Mol. Liq.* **2020**, *319*, 114168.
(48) Sellaoui, L.; Ali, J.; Badawi, M.; Bonilla-Petriciolet, A.; Chen, Z. Understanding the adsorption mechanism of Ag^{+} and Hg^{2+} on functionalized layered double hydroxide via statistical physics modeling. *Appl. Clay Sci.* **2020**, *198*, 105828.
(49) Ali, R. A.; Mobarak, M.; Badawy, A. M.; Lima, E. C.; Seliem, M. K.; Ramadan, H. S. New insights into the surface oxidation role in enhancing Congo red dye uptake by Egyptian ilmenite ore: experiments and physicochemical interpretations. *Surf. Interfaces.* **2021**, *26*, 101316.
(50) Mobarak, M.; Ali, R. A.; Seliem, M. K. Chitosan/activated coal composite as an effective adsorbent for Mn (VII): Modeling and interpretation of physicochemical parameters. *Int. J. Biol. Macromol.* **2021**, *186*, 750−758.
(51) Dhaouadi, F.; Sellaoui, L.; Reynel-Ávila, H. E.; Landín-Sandoval, V.; Mendoza-Castillo, D. I.; Jaime-Leal, J. E.; Lima, E. C.; Bonilla-Petriciolet, A.; Lamine, A. B. Adsorption mechanism of Zn^{2+}, Ni^{2+}, Cd^{2+}, and Cu^{+2} ions by carbon-based adsorbents: interpretation of the adsorption isotherms via physical modelling. *Environ. Sci. Pollut. Res.* **2021**, *28*, 30943−30954.
(52) Xiao, Y.; Hill, J. M. Solid acid catalysts produced by sulfonation of petroleum coke: Dominant role of aromatic hydrogen. *Chemosphere* **2020**, *248*, 125981.
(53) Poosumas, J.; Ngaosuwan, K.; Quitain, A. T.; Assabumrungrat, S. Role of ultrasonic irradiation on transesterification of palm oil using calcium oxide as a solid base catalyst. *Energy Convers. Manag.* **2016**, *120*, 62−70.
(54) Malani, R. S.; Patil, S.; Roy, K.; Chakma, S.; Goyal, A.; Moholkar, V. S. Mechanistic analysis of ultrasound-assisted biodiesel synthesis with Cu_2O catalyst and mixed oil feedstock using continuous (packed bed) and batch (slurry) reactors. *Chem. Eng. Sci.* **2017**, *170*, 743−755.
(55) Encinar, J. M.; Pardal, A.; Sánchez, N.; Nogales, S. Biodiesel by transesterification of rapeseed oil using ultrasound: a kinetic study of base-catalysed reactions. *Energies* **2018**, *11* (9), 2229.
(56) Tan, S. X.; Lim, S.; Ong, H. C.; Pang, Y. L. State of the art review on development of ultrasound-assisted catalytic transesterification process for biodiesel production. *Fuel* **2019**, *235*, 886−907.
(57) Wang, K.; Fu, J.; Wang, S.; Gao, M.; Zhu, J.; Wang, Z.; Xu, Q. Polydopamine-coated magnetic nanochains as efficient dye adsorbent with good recyclability and magnetic separability. *J. colloid Interface Sci.* **2018**, *516*, 263−273.
(58) Nasiri Azad, F.; Ghaedi, M.; Dashtian, K.; Hajati, S.; Goudarzi, A.; Jamshidi, M. Enhanced simultaneous removal of malachite green and safranin O by ZnO nanorod-loaded activated carbon: modeling, optimization and adsorption isotherms. *New J. Chem.* **2015**, *39*, 7998−8005.
(59) Sun, X. F.; Wang, S. G.; Liu, X. W.; Gong, W. X.; Bao, N.; Gao, B. Y.; Zhang, H. Y. Biosorption of Malachite Green from aqueous solutions onto aerobic granules: kinetic and equilibrium studies. *Bioresour. Technol.* **2008**, *99*, 3475−3483.
(60) Arellano-Cárdenas, S.; López-Cortez, S.; Cornejo-Mazón, M.; Mares-Gutiérrez, J. C. Study of malachite green adsorption by organically modified clay using a batch method. *Appl. Surf. Sci.* **2013**, *280*, 74−78.
(61) Kiani, G.; Dostali, M.; Rostami, A.; Khataee, A. R. Adsorption studies on the removal of malachite green from aqueous solutions onto halloysite nanotubes. *Appl. Clay Sci.* **2011**, *54*, 34−39.
(62) Awadallah-F, A. Adsorptive removal of malachite green chloride and reactive red-198 from aqueous solutions by using multiwall carbon nanotubes-graft-poly (2-acrylamido-2-methyl-1-propanesulfonic acid). *J. Polym. Environ.* **2017**, *25*, 258−276.
(63) Sartape, A. S.; Mandhare, A. M.; Jadhav, V. V.; Raut, P. D.; Anuse, M. A.; Kolekar, S. S. Removal of malachite green dye from aqueous solution with adsorption technique using Limonia acidissima (wood apple) shell as low cost adsorbent. *Arab. J. Chem.* **2017**, *10*, S3229−S3238.
(64) Janos, P. Sorption of Basic Dyes onto Iron Humate. *Environ. Sci. Technol.* **2003**, *37*, 5792.
(65) Raghu, M. S.; Yogesh Kumar, K.; Prashanth, M. K.; Prasanna, B. P.; Vinuth, R.; Pradeep Kumar, C. B. Adsorption and antimicrobial studies of chemically bonded magnetic graphene oxide-Fe_3O_4 nanocomposite for water purification. *J. Water Process. Eng.* **2017**, *17*, 22−31.

https://doi.org/10.1021/acsomega.2c04985
ACS Omega 2022, 7, 36697−36711